

Dieses Dokument ist eine Zweitveröffentlichung (Postprint) /

This is a self-archiving document (accepted version):

Min Hyuk Park, Ching-Chang Chung, Tony Schenk, Claudia Richter, Michael Hoffmann, Steffen Wirth, Jacob L. Jones, Thomas Mikolajick, Uwe Schroeder

Origin of Temperature-Dependent Ferroelectricity in Si-Doped HfO₂

Erstveröffentlichung in / First published in:

Advanced electronic materials. 2018, 13(9), Art.-Nr. 1700489 [Zugriff am: 24.08.2022]. Wiley. ISSN 2199-160X.

DOI: <https://doi.org/10.1002/aelm.201700489>

Diese Version ist verfügbar / This version is available on:

<https://nbn-resolving.org/urn:nbn:de:bsz:14-qucosa2-804981>

Origin of Temperature-Dependent Ferroelectricity in Si-Doped HfO₂

Min Hyuk Park, Ching-Chang Chung, Tony Schenk, Claudia Richter, Michael Hoffmann, Steffen Wirth, Jacob L. Jones, Thomas Mikolajick, and Uwe Schroeder*

The structural origin of the temperature-dependent ferroelectricity in Si-doped HfO₂ thin films is systematically examined. From temperature-dependent polarization-electric field measurements, it is shown that remanent polarization increases with decreasing temperature. Concurrently, grazing incidence X-ray diffraction shows an increase in the orthorhombic phase fraction with decreasing temperature. The temperature-dependent evolution of structural and ferroelectric properties is believed to be highly promising for the electrocaloric cooling application. Magnetization measurements do not provide any indication for a change of magnetization within the temperature range for the strong crystalline phase transition, suggesting that magnetic and structural properties are comparatively decoupled. The results are believed to provide the first direct proof of the strongly coupled evolution of structural and electrical properties with varying temperature in fluorite oxide ferroelectrics.

1. Introduction


Recently, fluorite-structure-based ferroelectric binary oxides have been gaining increasing interest due to their promising properties for various applications such as ferroelectric random access memories,^[1,2] ferroelectric field-effect transistors,^[2-4] negative capacitance field-effect transistors,^[5] pyroelectric energy harvesting,^[6-10] electrocaloric cooling,^[6-9] and electrostatic supercapacitors.^[11-15] This unexpected ferroelectricity was first reported in Si-doped HfO₂ thin films by Böske et al. in 2011.^[16] After this first paper, ferroelectricity has been observed in pure^[17,18]

Dr. M. H. Park, Dr. T. Schenk, C. Richter, M. Hoffmann,
Prof. T. Mikolajick, Dr. U. Schroeder
NaMLab gGmbH
Noethnitzer Str. 64, 01187 Dresden, Germany
E-mail: Uwe.Schroeder@namlab.com

Dr. C.-C. Chung, Prof. J. L. Jones
Department of Materials Science and Engineering
North Carolina State University
Raleigh, NC 27695-7907, USA

Dr. S. Wirth
Max-Planck-Institute for Chemical Physics of Solids
Noethnitzer Str. 40, 01187 Dresden, Germany

Prof. T. Mikolajick
Chair of Nanoelectronic Materials
TU Dresden
01062 Dresden, Germany

 The ORCID identification number(s) for the author(s) of this article can be found under <https://doi.org/10.1002/aelm.201700489>.

and doped HfO₂,^[4,16,19-27] Hf_{1-x}Zr_xO₂ (HZO),^[28-32] and ZrO₂^[33,34] thin films. It is now believed to originate from an orthorhombic phase with space group *Pca*2₁.^[16,35] The recently proven polar phase in extremely thin films implies a phase transition between the polar and the conventional nonpolar phase, which has not been observed in bulk materials. Generally, pyroelectric materials can have strong pyroelectricity at temperatures near the transition between a polar and a nonpolar (or another polar) phase.^[36,37] Consequently, a detailed understanding of the phase transition between these phases is of pivotal importance.

Böscke et al. observed a temperature-dependent change of polarization-electric field (*P-E*) characteristics of Si-doped HfO₂ thin films, and first reported a change of the *P-E* curve from a ferroelectric to an anti-ferroelectric-like shape with increasing temperature.^[38] Müller et al. investigated the temperature-dependent ferroelectric properties of HZO and ZrO₂ thin films down to 80 K, and confirmed a similar tendency.^[39] Park et al. comprehensively examined the temperature-dependent *P-E* characteristics of HZO thin films and suggested their application for electrocaloric cooling and energy harvesting.^[6] Hoffmann et al. also described similar phenomena in Si-doped HfO₂ thin films.^[7] According to these previous reports, the electrical properties of HZO and Si-doped HfO₂ thin films change from field-induced ferroelectric to ferroelectric with decreasing temperature, and this phenomenon is believed to originate from the phase transition of the tetragonal to the orthorhombic phase.^[6-9,39] Although it is believed that the structural and electrical properties of ferroelectric fluorites are strongly coupled, the strong coupling has not yet been directly confirmed upon varying the temperature of a single sample. Therefore, this study examines the temperature-dependent changes in structural and electrical properties of Si-doped HfO₂ thin films.

2. Results and Discussion

For the in situ temperature-dependent X-ray analysis, the doping concentration of Si-doped HfO₂ thin film needs to first be optimized. **Figure 1** shows the temperature-dependent changes in *P_r* of 40 nm thick Si-doped HfO₂ thin films with 4.5, 5.0, and 6.3 cat% Si doping concentration. For comparison, the data for 10 nm thick Si-doped HfO₂ from ref. ^[7] are also included. In a

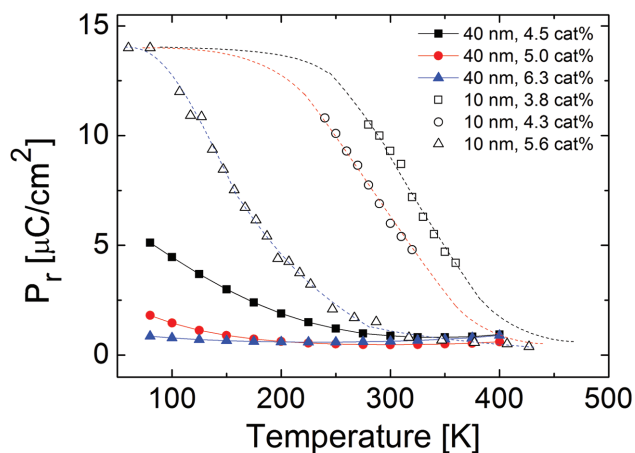


Figure 1. The temperature-dependent changes of remanent polarization (P_r) of 40 and 10 nm thick Si-doped HfO_2 thin films. The data for the 10 nm thick films are taken from ref. [7].

previous study,^[7] the temperature-dependent changes of polarization-electric field curves and the pyroelectric responses were comprehensively studied for 3.8–5.6 cat% Si-doped HfO_2 thin films. Thus, a similar doping concentration range (from 4.5 to 6.3 cat%) was examined for the 40 nm thick Si-doped HfO_2 films. The temperature-dependent P - E curves and the polarization-temperature (P - T) curves at various electric fields are included as Figures S1 and S2 (Supporting Information). It was reported that T_c decreases with increasing Si doping concentration, and the trend is also confirmed in the present study.^[7] Out of the

three samples, the 4.5 cat% Si-doped HfO_2 thin film showed the largest change in P_r values. As seen in Figure 1, the P_r of the 4.5 cat% Si-doped HfO_2 film increases from ≈ 0 to $5.1 \mu\text{C cm}^{-2}$ with decreasing T from 300 to 80 K. Although the maximum polarization is smaller compared to the 10 nm thick Si-doped HfO_2 thin films ($12\text{--}14 \mu\text{C cm}^{-2}$), this result implies the partial tetragonal to orthorhombic phase transition with decreasing temperature for the 4.5 cat% Si-doped HfO_2 thin film. The effect of film thickness on the phase transition is not clearly understood currently and requires further study. It should also be noted that the maximum P_r value achievable by optimizing doping concentration decreases with increasing film thickness.^[40] We recently examined the effect of Si doping concentration on the ferroelectric properties for 36 nm thick HfO_2 films,^[40] and the doping concentration of 4.5 cat% was the boundary between field-induced ferroelectric and ferroelectric properties. The P_r rapidly increases to over $9 \mu\text{C cm}^{-2}$ ($>70\%$ of the maximum achievable P_r for 36 nm thick films) by slightly decreasing Si concentration from 4.5% to 4.1%. For ferroelectric Si-doped HfO_2 thin films, it is well known that the P - E curve is pinched in the pristine state before any electric characterization possibly due to an internal bias field, pinning of domains, or the formation of a secondary nonferroelectric phase.^[41–43] Thus, the pinched hysteresis needs to be distinguished from double hysteresis loop as expected for a field-induced phase transition.^[44] The stability of the antiferroelectric hysteresis resulting from the field-induced phase transition was experimentally confirmed by Hoffmann et al. using first-order reversal curve measurements.^[45] Thus, the lower Si doping concentration is not expected to show strong temperature-dependent phase transition within the temperature range

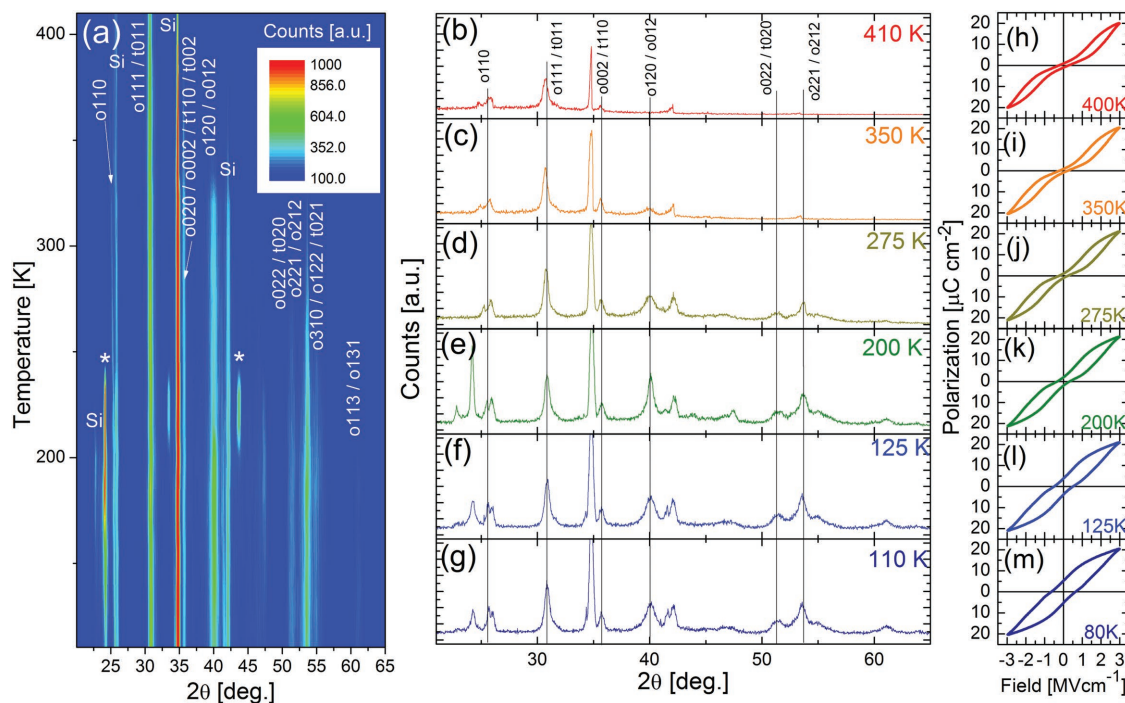


Figure 2. a) An intensity contour map of grazing incidence X-ray diffraction (GIXRD) patterns of 40 nm thick 4.5 cat% Si-doped HfO_2 films measured in a temperature range from 110 to 410 K (*: unknown peaks). The GIXRD patterns of 40 nm thick 4.5 cat% Si-doped HfO_2 films measured at b) 410, c) 350, d) 275, e) 200, f) 125, and g) 110 K, respectively. The polarization-electric field (P - E) curves of 40 nm thick 4.5 cat% Si-doped HfO_2 films measured at h) 400, i) 350, j) 275, k) 200, l) 125, and m) 80 K, respectively.

tested in this study. Moreover, Müller and co-workers examined the effect of temperature on the ferroelectric properties of ferroelectric Si-doped HfO₂ thin film. No decrease in P_r could be observed with increasing temperature up to 470 K, which is 70 K higher than the maximum temperature used in this study.^[46]

Figure 2a shows the intensity contour map constructed from temperature-dependent grazing incidence X-ray diffraction (GIXRD) patterns of a 40 nm thick 4.5 cat% Si-doped HfO₂ thin film measured from 110 to 410 K. After the sample was first cooled down to 110 K, GIXRD measurements were conducted every 15 K with increasing temperature. Since too low of diffraction intensities are expected for ≈ 10 nm thick films, as in most of the previous studies, we chose a 40 nm thick film in this study. Figure 2b–g exhibits the GIXRD patterns measured at 410, 350, 275, 200, 125, and 110 K, respectively, in more detail. From Figure 2a,b, it could be noticed that the monoclinic phase is not formed, which can be proven by the absence of the 111 (at $\approx 31.5^\circ$) and -111 (at $\approx 28.5^\circ$) diffraction peaks. Since the lattice parameters of the orthorhombic and tetragonal phase are almost equal, it is nearly impossible to distinguish these two phases just from the lattice parameters alone. However, due to the difference in their symmetry, the orthorhombic phase can have characteristic diffraction peaks that are forbidden for the tetragonal phase. Mueller and Park suggested that the 221 diffraction peak can be considered as a characteristic sign of the orthorhombic phase distinguished from both monoclinic and tetragonal phases.^[47,48] Shimizu et al. conducted a wide-area reciprocal space mapping on their epitaxial Y-doped HfO₂ thin films, showing that the orthorhombic phase can have several superspots (from 110, 201, and 211 diffraction peaks), which are forbidden in the tetragonal phase.^[49] Based on the suggestions in previous studies, the expected angles of diffraction peaks from the orthorhombic and the tetragonal Si-doped HfO₂ films were systematically analyzed based on the lattice parameters reported in previous studies.^[16,35,47–52] As a result, among the four characteristic diffraction peaks suggested previously, o110 ($\approx 25^\circ$) and o120/o012/o201 ($\approx 40^\circ$, this peak will be called o120 peak afterward for the sake of convenience) were chosen to distinguish the orthorhombic phase from the tetragonal phase. As seen in Figure 2b, the o110 and o120 diffraction peaks are barely observed at 410 K, but with decreasing temperature to 350 K, a weak o120 diffraction peak begins to emerge. The intensity of the o120 peak increases with further decreasing temperature below 350 K as seen in Figure 2c–g. For the case of the o110 diffraction peak ($\approx 25^\circ$), a very weak peak can be identified on the left shoulder of the Si substrate diffraction peak ($\approx 26^\circ$). The GIXRD patterns of the Si substrate and the sample holder were also measured and are included as Figure S3 (Supporting Information) to exclude any false assignments of peaks. The o110 diffraction peak is clearly observed with further decreasing temperature from 200 K as seen in Figure 2e–g. These temperature-dependent GIXRD results suggest that the partial phase transition of this Si-doped HfO₂ film from the tetragonal to the orthorhombic is noticeable below 350 K.

In Figure 2h–m, the P - E curves measured at 400, 350, 275, 200, 125, and 80 K, respectively, are presented. As seen in Figure 2h–j, the Si-doped HfO₂ film shows a characteristic double hysteresis that is believed to originate from the field-induced phase transition between the tetragonal and the orthorhombic phase.

Pinning of domains is another potential cause for a pinched P - E hysteresis. Based on the changes in electric field required for the transition with varying temperature and doping concentrations.^[6–9] in HfO₂ thin films with rather high doping concentrations the field-induced phase transition is generally accepted as the cause of the pinched hysteresis. The same trend can be derived based on theoretical calculations.^[45] With further decreasing temperature below 200 K, an increase in the remanent polarization (P_r) value could be clearly confirmed. This implies that the tetragonal to orthorhombic phase transition is expected from the electrical characterization.

To compare the temperature-dependent changes in GIXRD and P - E curves, the intensities of the o110 and o120 diffraction peaks were normalized by the intensity of the o111/t011 diffraction peak. These changes of normalized intensities of the o110 and o120 diffraction peaks are depicted in Figure 3a,b, respectively. Clearly, the normalized intensities of the o110 and o120 diffraction peaks increase with decreasing temperature, suggesting an increase in the orthorhombic phase fraction in the film. The temperature-dependent lattice parameters were also calculated from the XRD patterns measured in Bragg–Brentano geometry at various temperatures. To avoid misalignment issues during the GIXRD measurement, the lattice parameters were calculated from in situ Bragg–Brentano XRD results, and the intensity contour map of the temperature-dependent normal XRD is included as Figure S4 (Supporting Information). Figure 3c shows the lattice parameters a , b , and c calculated from the angles of o111/t011 and o002/o020/t200 diffraction peaks in the normal XRD patterns. Since the lattice parameters b and c cannot be clearly distinguished due to their similar magnitude, only their average is calculated and plotted in Figure 3c. It should be noted that the lattice parameters of double sized tetragonal unit cell were calculated for a fair comparison between the tetragonal and orthorhombic phases. Figure 3d shows the aspect ratio ($2a/(b+c)$) for the orthorhombic and c/a for the tetragonal phase) as derived from Figure 3c and the corresponding unit cell volume. The unit cell volume slightly decreases with decreasing temperature, as can be expected from the lattice parameter changes in Figure 3c. On the other hand, the aspect ratio remained reasonably constant at ≈ 0.994 exhibiting only slight fluctuations with temperature. Figure 3d shows, given the changing fractions of the orthorhombic and tetragonal phases, that the difference in the aspect ratio of the orthorhombic and tetragonal phases is negligible, whereas all the lattice parameters are linearly dependent on temperature.

It was recently reported that the change of the aspect ratio is a sign of phase change when the doping concentration varies, but such a change could not be observed with varying temperature in the same study.^[50] Instead, the aspect ratio of the lattice parameters in Si-doped HfO₂ decreased from 1.02 to 0.99 with increasing Si doping concentration, which was well matched with the change of P_r and the orthorhombic phase fraction from Rietveld refinement.^[50] Therefore, the aspect ratio was suggested as an important sign for the phase change with varying doping concentration.^[50] It is believed that for the case of a temperature-dependent phase evolution the change of lattice parameters is negligible possibly due to the constraint effect from the substrate and electrodes. From the P - E curves

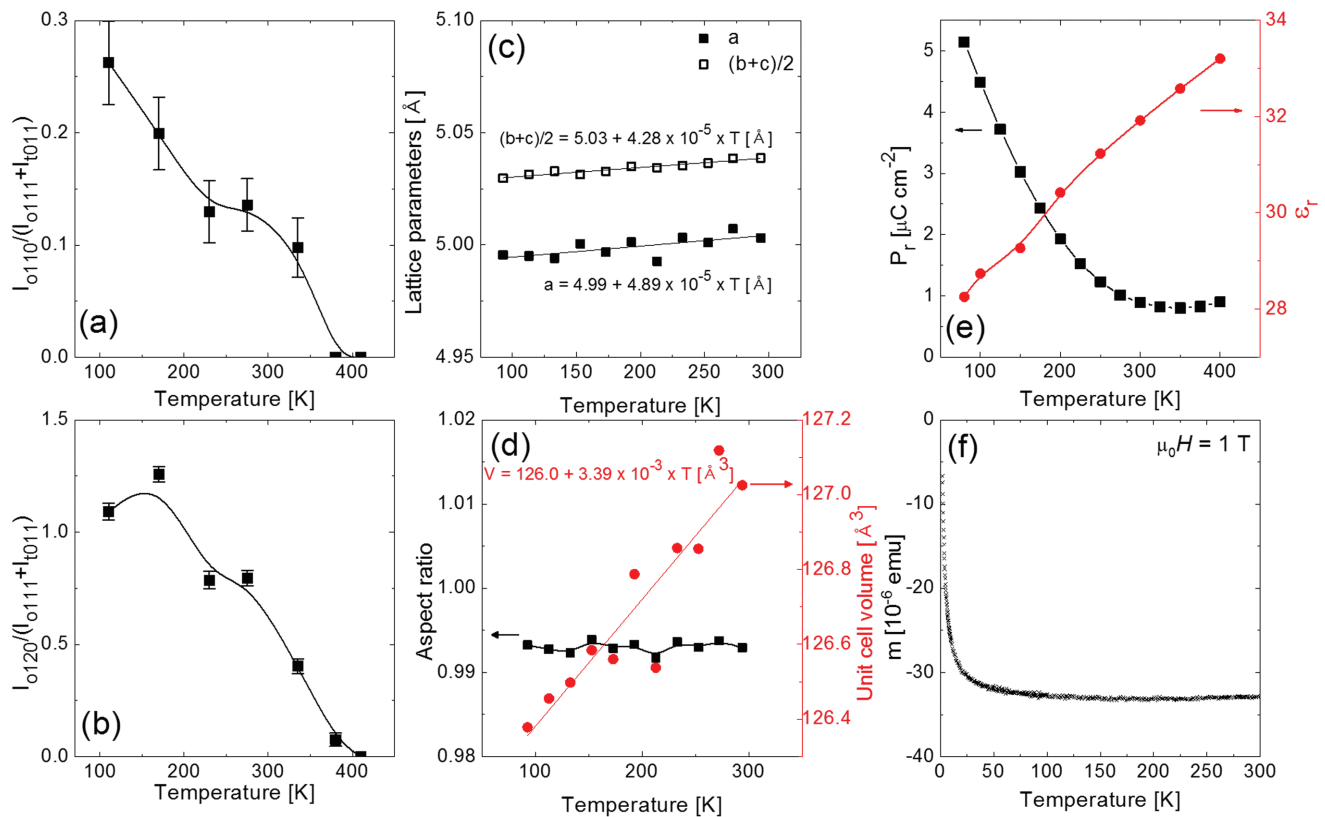


Figure 3. The normalized intensities of a) orthorhombic 110 (σ_{110}) and b) 120 (σ_{120}) diffraction peaks measured at various temperatures. The error bars in (a) and (b) were determined from the areal errors in Gaussian fitting results. c) The lattice parameters, d) the aspect ratio ($2a/(b+c)$ for orthorhombic and c/a for tetragonal phase), and the unit cell volume calculated from the temperature-dependent XRD data measured within Bragg-Brentano geometry. The black lines in (c) and the red line in (d) show the linear fitting of the data. e) The remanent polarization (P_r , left y -axis) and dielectric constant (ϵ_r , right y -axis) values and f) the magnetization value m measured at various temperatures. The lines in (a), (b), and (e) are just guides to the eyes.

presented in Figure 2h–m, it can be noticed that the tetragonal to orthorhombic phase transition occurs only for a small fraction of the Si-doped HfO_2 thin film, since the P_r at 80 K is still about $5.1 \mu\text{C cm}^{-2}$ and not saturated. Therefore, the lattice parameter of the orthorhombic phase should be strongly affected by the adjacent tetragonal phase. This might be the reason why the lattice parameters, the aspect ratio, and the unit cell volume even at the lowest temperature are rather similar to those of the high-temperature tetragonal phase in this study. The coefficient of thermal expansion (CTE) of Si-doped HfO_2 , which is estimated from the linear fitting of the lattice parameters' change, is about 9.8×10^{-6} and $8.5 \times 10^{-6} \text{ K}^{-1}$ for a and $(b+c)/2$. The CTEs are smaller compared to the values in the literature when they are compared to the CTEs measured for tetragonal HfO_2 at high temperatures.^[52] Haggerty et al. measured the CTE of tetragonal HfO_2 in the temperature range of 1350–1850 °C, and the CTEs of a and c -axes were $8.4\text{--}11.24 \times 10^{-6} \text{ K}^{-1}$ and $12.5\text{--}16.90 \times 10^{-6} \text{ K}^{-1}$, respectively.^[52] However, it was reported that the CTE of HfO_2 decreases with increasing Si doping concentration and decreasing temperature.^[53] Since the thermal expansion in thin film is strictly limited by that of substrate, moreover, the CTE of thin film estimated from the temperature-dependent XRD can be estimated differently from its intrinsic CTE. It is believed that the grains of Si-doped HfO_2

thin film used in this study should have almost random orientation as previously reported by Schenk.^[54] These results indicate that the structural evolution in Si-doped HfO_2 thin films is generally governed by the sub-unit cell motion of Hf and O ions rather than the lattice parameters' change. From the relative position of Hf and O, the motion of O should be much stronger compared to that of Hf.^[51]

Figure 3e shows the temperature-dependent change of P_r (black square symbols) and the dielectric constant (ϵ_r , red circle symbols) values. As mentioned before the P_r is only $\approx 5.1 \mu\text{C cm}^{-2}$ even at the lowest temperature of 80 K, which is only 20.2 % of the theoretical P_r ($\approx 25.2 \mu\text{C cm}^{-2}$) of randomly oriented polycrystalline orthorhombic HfO_2 film.^[55] This discrepancy suggests that the Si-doped HfO_2 thin film was only partially transformed into the ferroelectric phase. This might be the reason why the intensities of characteristic diffraction peaks from the orthorhombic phase are quite weak even at 80 K. However, 80 K is the lower limit of our measurement system that can be cooled down using liquid N_2 . The ϵ_r value linearly decreases from 33 to 28 with decreasing temperature from 400 to 80 K. The ϵ_r value was measured using an impedance spectroscopy, and the details of the analysis can be found in a previous study and in the Experimental Section.^[56] To determine the appropriate AC voltage amplitude, a impedance spectroscopy

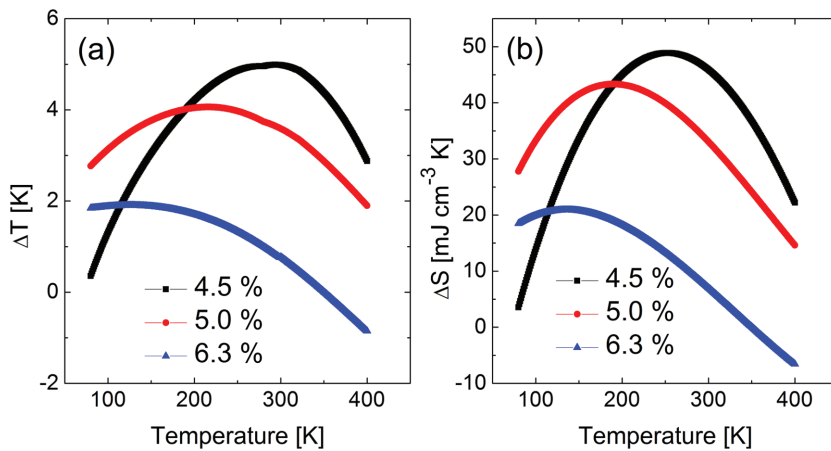


Figure 4. a) The adiabatic temperature change (ΔT) and b) the isothermal entropy change (ΔS) of 40 nm thick 4.5, 5.0, and 6.3 cat% Si-doped HfO_2 films calculated from temperature-dependent changes in polarization.

measurement with various AC voltage amplitudes was tested, and the amplitude of 200 mV was chosen for this study. The impedance spectra with various AC voltage amplitude will be published elsewhere with a systematic study of the Rayleigh behavior in Si-doped HfO_2 thin films.^[56] It was reported that the impedance spectroscopy can be an effective tool to examine the dielectric and ferroelectric properties in doped HfO_2 thin films.^[57,58] The equivalent circuit considered and the resulting parameters are summarized in Figure S5 and Table S1 (Supporting Information). Interestingly, the abrupt ϵ_r increase according to the Curie–Weiss law could not be observed.^[59] It is believed that this is due to the wide distribution of the grain size and resulting broad distribution of Curie (T_c) or Curie–Weiss temperature (T_0) reported in previous studies.^[7,9] It is generally known that the phase transition in polycrystalline thin films or nanocrystallites is broader compared to their bulk or epitaxial thin film counterparts.^[60,61] Our Si-doped HfO_2 thin film should be the extreme case with a very wide distribution of T_c , a fact that is also corroborated by the P_r change seen in Figure 3e. For HfO_2 thin films doped with various dopants, such extremely wide phase transition was already reported before.^[6–9] Furthermore, in Figure 3, compared to the change of the normalized intensity of o110 and o120 diffraction peaks, the rapid increase of P_r seems to continue to temperatures even lower than 80 K. It should be noted that a partial phase transition does not necessarily guarantee that a clear polarization switching can be observed. Although a small fraction of the film exists in the ferroelectric phase, the polarization switching could be suppressed by the large fraction of the nonferroelectric phase. It was reported that the grain size distribution may cause a wide distribution of T_c ,^[7] and it was also suggested that the inhomogeneous distribution of the dopants and oxygen vacancies can affect the T_c distribution.^[9] Tagantsev et al. reported that even very thin nonferroelectric layers can strongly suppress the polarization switching in ferroelectric thin films.^[62]

In addition to our structural and ferroelectrical studies, the magnetic properties were investigated to check for the possibility of multiferroic properties of Si-doped HfO_2 thin films. In

principle, HfO_2 can never be ferromagnetic without the involvement of defect-related mechanisms since there are otherwise no unpaired electrons in its orbitals.^[63] Indeed, it was suggested that HfO_2 could show ferromagnetic properties due to defects such as oxygen vacancies both from experiment and computational calculation.^[63,64] On the other hand, it was also proposed that the ferromagnetic properties in HfO_2 may simply originate from a contamination effect from stainless steel tweezers.^[65] Figure 3f shows the temperature-dependent change of magnetization of a 4.5 cat% Si-doped HfO_2 thin film. As seen in the figure, no change in the magnetization could be observed within the temperature range of interest. A weak hysteresis could be detected at extremely low temperatures (see Figure S6 in the Supporting Information), but it likely

originates from impurities or other artifacts. Therefore, it is believed that at least the present sample, if not all HfO_2 -based ferroelectrics, does not exhibit multiferroic properties.

Figure 4a,b shows the adiabatic temperature change (ΔT) and ΔS of the 40 nm thick Si-doped HfO_2 films. The ΔT and ΔS values were calculated using Equations (1) and (2)

$$\Delta T = -\frac{1}{\rho C} \int_{E_1}^{E_2} T \left(\frac{\partial P}{\partial T} \right)_E dE \quad (1)$$

$$\Delta S = -\frac{1}{\rho} \int_{E_1}^{E_2} \left(\frac{\partial P}{\partial T} \right)_E dE \quad (2)$$

In Equations (1) and (2), ρ and C are the density and specific heat, respectively. These equations are based on the Maxwell relation $(\partial P/\partial T)_E = (\partial S/\partial E)_T$. A fourth-order polynomial was used to fit the P - T data, and the specific heat value as a function of temperature was taken from the literature.^[66] The theoretical density was calculated from the lattice parameters in Materlik and co-workers' previous study, Ref. [51] and the calculated density was 10.7 g cm^{-3} . The electric field range from 0.0 to 3.0 MV cm^{-1} was used for the calculation of ΔT and ΔS . As seen in Figure 4a,b, the temperature for maximum ΔT and ΔS decreases with increasing Si doping concentration. This Si doping concentration dependency is consistent with that in a previous study.^[7] The maximum ΔT values are 5.0 K (at 294 K), 4.1 K (at 216 K), and 1.9 K (at 126 K) for 4.5, 5.0, and 6.3 cat% Si-doped HfO_2 thin films, respectively. It should be noted that the negative ΔT and ΔS values for 6.3 cat% Si-doped HfO_2 in Figure 4b are assumed to be an artifact due to rather small temperature-dependent changes in polarization values. The maximum ΔT value of 4.5 cat% Si-doped HfO_2 films is about 53% of the largest ΔT value ($\approx 9.5 \text{ K}$) ever reported for a 9 nm thick 5.6 cat% Si-doped HfO_2 film.^[7] However, since the film thickness used in this study is 4.4 times larger than that in the previous study,^[7] the practical cooling capacity per area can be 2.3 times larger when capacitors with equivalent area are compared.

It should be noted that this work examined the electrocaloric effect of 40 nm thick fluorite ferroelectric films for the

first time. For practical applications, the scaling-up of film thickness is a very important task for fluorite structured ferroelectric films. For both Si-doped HfO₂ and HZO thin films, it was reported that the monoclinic phase fraction significantly increased with increasing film thickness.^[67,68] In contrast to a previous study by Yurchuk et al., the monoclinic phase formation could be effectively suppressed in our films, suggesting that the scale-up of fluorite ferroelectrics is possible by optimizing process parameters.^[49,67] Starschich et al. reported that the monoclinic phase formation can be suppressed for doped HfO₂ or ZrO₂ films deposited by using chemical solution deposition.^[24,25,34] Especially for pure ZrO₂ thin films, a strong ferroelectricity could be observed even up to 390 nm thickness.^[33] Richter et al.^[40] reported that the monoclinic phase fraction can be significantly lowered even with atomic layer deposition (ALD) different from Yurchuk et al.'s work.^[67] Kim et al. found that the formation of the monoclinic phase in Hf_{0.5}Zr_{0.5}O₂ thin films can be prevented by decreasing the deposition temperature for their atomic layer deposition process.^[14] These studies show that the newly found fluorite ferroelectrics are one of the most promising materials for electrocaloric cooling applications as well as energy harvesting and storage.

3. Conclusion

In conclusion, the strongly coupled evolution of structural and electrical properties of the newly found fluorite ferroelectrics is directly proven on a single sample with varying temperature for the first time. From the changes in the intensities of characteristic diffraction peaks of the orthorhombic phase and changes in *P-E* curves measured within a wide range of temperature, strong coupling could be clearly confirmed. Magnetization measurements confirmed the absence of strong temperature dependence. Moreover, the electrocaloric effect of 40 nm thick fluorite ferroelectric films is examined for the first time. An adiabatic temperature change ΔT of 5.0 K could be observed for the 40 nm thick 4.5 cat% Si-doped HfO₂ thin film. Although the maximum ΔT is smaller than the largest-ever value (9.5 K) reported for Si-doped HfO₂ thin films, the practical cooling capacity per area is expected to be 2.3 times larger.

4. Experimental Section

Sample Preparation: Si-doped HfO₂ films were deposited by ALD in an Oxford Instruments OpAL ALD tool. Tetrakis[ethylmethylamino]hafnium (TEMA-Hf) and *N,N,N',N'*-tetraethylsilanediamine (SAM.24) were used as metalorganic precursors for HfO₂ and SiO₂, respectively. H₂O and O₂ plasma were used as oxygen sources for HfO₂ and SiO₂, respectively. The ALD cycle ratio between SiO₂ and HfO₂ was 1:20, and the expected cationic ratio of Si/(Hf+Si) is 4.5 cat%. The substrate temperature for the ALD process was 280 °C. Postmetallization annealing was performed in an AST rapid thermal processing tool under at 800 °C N₂ atmosphere for 10 min. 12 nm thick TiN top and bottom electrodes were sputtered in an Alliance Concept CT200 physical vapor deposition tool. To crystallize the Si-doped HfO₂ thin film, it was annealed using a rapid thermal process with a ramp rate of 33 °C s⁻¹ at 800 °C for 10 min in N₂ atmosphere after sputtering of TiN top electrode. The 25 nm thick Pt pads as well as 10 nm thick Ti adhesion layer were deposited using e-beam evaporation and were patterned using a shadow mask. The Pt electrodes served as an etch stopper

when TiN top electrodes were selectively etched afterward in a diluted SC1 solution (H₂O:H₂O₂:NH₄OH in a ratio of 50:2:1 at 50 °C). The experimental details of sample fabrication can be found in a previous study.^[40]

Electrical Characterization: A triangular voltage was applied to the bottom electrode while the top electrode was connected to virtual ground, and a measurement frequency of 1 kHz was used. The *P_r* values for doped HfO₂ films were taken from the *P-E* curves achieved with 3.0 MV cm⁻¹ maximum field amplitude. For low-temperature measurements, a probe station equipped with a chamber that can be evacuated down below 1.3 × 10⁻⁴ Pa was used. The sample stage in the chamber was cooled down using liquid nitrogen. Impedance spectroscopy was conducted with an HP 4294A (Agilent Technologies). A small-signal amplitude of 200 mV and a point averaging factor of 25 were applied. Details about the choice of the equivalent circuit as well as about the fitting procedure can be found in our previous study.^[55]

Structural Analysis: The crystal structures of the samples were analyzed using an X-ray diffractometer (Empyrean, PANalytical) with a low-temperature chamber (TTK450, Anton Paar) and a Cu-K α X-ray source in a temperature of 110–410 K. The samples were cooled to 110 K with a cooling rate of 10 K min⁻¹ without collecting diffraction patterns. After that, GIXRD patterns were acquired with a grazing incidence angle of 1.5° 2θ in a range of 20–65° every 15 K from 110 to 410 K. The step size and count time for the GIXRD measurements were 0.026° and 84.2 s per step, respectively. To be noted that, the z-location of the sample was realigned and the sample was held for additional 5 min prior to each measurement. For the lattice parameters' estimation, the in situ XRD measurement was repeated again using a Bragg–Brentano geometry.

Magnetic Characterization: Magnetization measurements were conducted using a commercial magnetic properties measurement system (MPMS by Quantum Design, Inc.). Empty quartz sample holders were evaluated before mounting the sample to minimize its background signal. Subsequently, the thin film samples were mounted such that the magnetic field (of maximum 5 T) was applied in an in-plane geometry.

Supporting Information

Supporting Information is available from the Wiley Online Library or from the author.

Acknowledgements

The authors gratefully acknowledge funding from Army Research Office (Contract No. W911NF-15-1-0593). T.S. gratefully thanks the German Research Foundation (Deutsche Forschungsgemeinschaft) for funding part of this research in the frame of the "Inferox" project (MI 1247/11-2). M.H.P. was supported by Humboldt postdoctoral fellowship from the Alexander von Humboldt Foundation. M.H.P. acknowledges Basic Science Research Program through the National Research Foundation of Korea (NRF) funded by the Ministry of Education (2016R1A6A3A03012208). This work was performed in part at the Analytical Instrumentation Facility (AIF) at North Carolina State University, which is supported by the State of North Carolina and the National Science Foundation (Award No. ECCS-1542015). The AIF is a member of the North Carolina Research Triangle Nanotechnology Network (RTNN), a site in the National Nanotechnology Coordinated Infrastructure (NNCI).

Conflict of Interest

The authors declare no conflict of interest.

Keywords

ferroelectricity, hafnia, phase transition, pyroelectricity, structural analysis

Received: October 11, 2017
Revised: November 15, 2017
Published online:

- [1] S. Mueller, S. R. Summerfelt, J. Müller, U. Schroeder, T. Mikolajick, *Electron Device Lett.* **2012**, 33, 1300.
- [2] T. Mikolajick, S. Müller, T. Schenk, E. Yurchuk, S. Slesazek, U. Schröder, S. Flachowsky, R. van Bentum, S. Kolodinski, P. Polakowski, J. Müller, *Adv. Sci. Technol.* **2014**, 95, 136.
- [3] J. Müller, E. Yurchuk, J. Paul, R. Hoffmann, S. Müller, D. Martin, S. Slesazek, P. Polakowski, J. Sundqvist, M. Czernohorsky, K. Seidel, P. Kücher, R. Boschke, M. Trentzsch, K. Gebauer, U. Schröder, T. Mikolajick, *Symp. on VLSI Technology Digest of Technical Papers*, IEEE, Honolulu, HI **2012**, p. 25.
- [4] J. Müller, T. S. Böske, Y. Yurchuk, P. Polakowski, J. Paul, D. Martin, T. Schenk, K. Khullar, A. Kersch, W. Weinreich, S. Riedel, K. Seidel, A. Kumar, T. M. Arruda, S. V. Kalinin, T. Schlosser, R. Boschke, R. van Bentum, U. Schröder, T. Mikolajick, in *Technical Digest - International Electron Devices Meeting*, IEEE, USA **2013**, pp. 10.8.1–10.8.4.
- [5] M. Hoffmann, M. Pešić, K. Chatterjee, A. I. Khan, S. Salahuddin, S. Slesazek, U. Schroeder, T. Mikolajick, *Adv. Funct. Mater.* **2016**, 26, 8643.
- [6] M. H. Park, H. J. Kim, Y. J. Kim, T. Moon, K. D. Kim, C. S. Hwang, *Nano Energy* **2015**, 12, 131.
- [7] M. Hoffmann, U. Schroeder, C. Küneth, A. Kersch, S. Starschich, U. Böttger, T. Mikolajick, *Nano Energy* **2015**, 18, 154.
- [8] M. H. Park, H. J. Kim, Y. J. Kim, T. Moon, K. D. Kim, Y. H. Lee, S. D. Hyun, C. S. Hwang, *Adv. Mater.* **2016**, 28, 7956.
- [9] M. H. Park, T. Schenk, M. Hoffmann, S. Knebel, J. Gartner, T. Mikolajick, U. Schroeder, *Nano Energy* **2017**, 36, 381.
- [10] S. W. Smith, A. R. Kitahara, M. A. Rodriguez, M. D. Henry, M. T. Brumbach, J. F. Ihlefeld, *Appl. Phys. Lett.* **2017**, 110, 072901.
- [11] M. H. Park, H. J. Kim, Y. J. Kim, T. Moon, K. D. Kim, C. S. Hwang, *Adv. Energy Mater.* **2014**, 4, 201400610.
- [12] M. Pešić, M. Hoffmann, C. Richter, T. Mikolajick, U. Schroeder, *Adv. Funct. Mater.* **2016**, 26, 7486.
- [13] P. D. Lomenzo, C.-C. Chung, C. Zhou, J. L. Jones, T. Nishida, *Appl. Phys. Lett.* **2017**, 110, 232904.
- [14] K. D. Kim, Y. H. Lee, T. Gwon, Y. J. Kim, H. J. Kim, T. Moon, S. D. Hyun, H. W. Park, M. H. Park, C. S. Hwang, *Nano Energy* **2017**, 39, 390.
- [15] M. H. Park, Y. H. Lee, H. J. Kim, Y. J. Kim, T. Moon, K. D. Kim, J. Müller, A. Kersch, U. Schroeder, T. Mikolajick, C. S. Hwang, *Adv. Mater.* **2015**, 27, 1811.
- [16] T. S. Böske, J. Müller, D. Bräuhaus, U. Schröder, U. Böttger, *Appl. Phys. Lett.* **2011**, 99, 102903.
- [17] P. Polakowski, J. Müller, *Appl. Phys. Lett.* **2015**, 106, 232905.
- [18] K. D. Kim, M. H. Park, H. J. Kim, Y. J. Kim, T. Moon, Y. H. Lee, S. D. Hyun, T. Gwon, C. S. Hwang, *J. Mater. Chem. C* **2016**, 4, 6484.
- [19] J. Müller, U. Schröder, T. S. Böske, I. Müller, U. Böttger, L. Wilde, J. Sundqvist, M. Lemberger, P. Kücher, T. Mikolajick, L. Frey, *J. Appl. Phys.* **2011**, 110, 114113.
- [20] S. Mueller, J. Mueller, A. Singh, S. Riedel, J. Sundqvist, U. Schroeder, T. Mikolajick, *Adv. Funct. Mater.* **2012**, 22, 2412.
- [21] S. Mueller, C. Adelman, A. Singh, S. Van Elshocht, U. Schroeder, T. Mikolajick, *ECS J. Solid State Sci. Technol.* **2012**, 1, N123.
- [22] T. Schenk, S. Mueller, U. Schroeder, R. Materlik, A. Kersch, M. Popovici, C. Adelman, S. Van Elshocht, T. Mikolajick, in *2013 Proc. of the European Solid-State Device Research Conf. (ESSDERC)*, IEEE, New York **2014**, p. 260.
- [23] U. Schroeder, S. Mueller, J. Mueller, E. Yurchuk, D. Martin, C. Adelman, T. Schloesser, R. van Bentum, T. Mikolajick, *Jpn. J. Appl. Phys.* **2013**, 2, N69.
- [24] S. Starschich, D. Griesche, T. Schneller, U. Böttger, *ECS J. Solid State Sci. Technol.* **2015**, 4, P419.
- [25] S. Starschich, U. Boettger, *J. Mater. Chem. C* **2017**, 5, 333.
- [26] L. Xu, T. Nishimura, S. Shibayama, T. Yajima, S. Migita, A. Toriumi, *Appl. Phys. Express* **2016**, 9, 091501.
- [27] A. G. Chernikova, D. S. Kuzmichev, D. V. Negrov, M. G. Kozodaev, S. N. Polyakov, A. M. Markeev, *Appl. Phys. Lett.* **2016**, 108, 242905.
- [28] J. Müller, T. S. Böske, D. Bräuhaus, U. Schröder, U. Böttger, J. Sundqvist, P. Kücher, T. Mikolajick, L. Frey, *Appl. Phys. Lett.* **2011**, 99, 112901.
- [29] M. H. Park, H. J. Kim, Y. J. Kim, W. Lee, T. Moon, C. S. Hwang, *Appl. Phys. Lett.* **2013**, 102, 242905.
- [30] J. Müller, T. S. Böske, U. Schröder, S. Mueller, D. Bräuhaus, U. Böttger, L. Frey, T. Mikolajick, *Nano Lett.* **2012**, 12, 4318.
- [31] M. H. Park, H. J. Kim, Y. J. Kim, T. Moon, C. S. Hwang, *Appl. Phys. Lett.* **2014**, 104, 072901.
- [32] H. Yu, C.-C. Chung, N. Shewmon, S. Ho, J. H. Carpenter, R. Larrabee, T. Sun, J. L. Jones, H. Ade, B. T. O'Connor, F. So, *Adv. Funct. Mater.* **2017**, 27, 1700461.
- [33] S. Starschich, T. Schenk, U. Schroeder, U. Boettger, *Appl. Phys. Lett.* **2017**, 110, 182905.
- [34] B.-T. Lin, Y.-W. Lu, J. Shieh, M.-J. Chen, *J. Eur. Ceram. Soc.* **2017**, 37, 1135.
- [35] X. Sang, E. D. Grimley, T. Schenk, U. Schroeder, J. M. LeBeau, *Appl. Phys. Lett.* **2015**, 106, 162905.
- [36] A. S. Mischenko, Q. Zhang, J. F. Scott, R. W. Whatmore, N. D. Mathur, *Science* **2006**, 311, 1270.
- [37] B. Neese, B. Chu, S.-G. Lu, Y. Wang, E. Furman, Q. M. Zhang, *Science* **2008**, 321, 821.
- [38] T. S. Böske, St. Teichert, D. Bräuhaus, J. Müller, U. Schröder, U. Böttger, T. Mikolajick, *Appl. Phys. Lett.* **2011**, 99, 102903.
- [39] M. H. Park, H. J. Kim, Y. H. Lee, Y. J. Kim, T. Moon, K. D. Kim, S. D. Hyun, C. S. Hwang, *Nanoscale* **2016**, 8, 13898.
- [40] C. Richter, T. Schenk, M. H. Park, F. A. Tschamtko, E. D. Grimley, J. M. LeBeau, C. Zhou, C. M. Fancher, J. L. Jones, T. Mikolajick, U. Schroeder, *Adv. Electron. Mater.* **2017**, 3, 1700131.
- [41] T. Schenk, M. Hoffmann, J. Ocker, M. Pešić, T. Mikolajick, U. Schroeder, *ACS Appl. Mater. Interfaces* **2015**, 7, 20224.
- [42] D. Zhou, J. Xu, Q. Li, Y. Guan, F. Cao, X. Dong, J. Müller, T. Schenk, U. Schröder, *Appl. Phys. Lett.* **2013**, 103, 192904.
- [43] M. H. Park, H. J. Kim, Y. J. Kim, T. Moon, K. D. Kim, S. D. Hyun, F. Fengler, U. Schroeder, C. S. Hwang, *ACS Appl. Mater. Interfaces* **2016**, 8, 15466.
- [44] T. Schenk, E. Yurchuk, S. Mueller, U. Schroeder, S. Starschich, U. Böttger, *Appl. Phys. Rev.* **2014**, 1, 041103.
- [45] M. Hoffmann, T. Schenk, M. Pešić, U. Schroeder, T. Mikolajick, *Appl. Phys. Lett.* **2017**, 111, 182902.
- [46] S. Mueller, J. Mueller, U. Schroeder, T. Mikolajick, *IEEE Trans. Device Mater. Reliab.* **2013**, 13, 93.
- [47] J. Mueller, *PhD Thesis*, TU Dresden, Germany **2014**.
- [48] M. H. Park, *PhD Thesis*, Seoul National University, Seoul, Korea **2014**.
- [49] T. Shimizu, K. Katayama, T. Kiguchi, T. J. Konno, O. Sakata, H. Funakubo, *Sci. Rep.* **2016**, 6, 32931.
- [50] M. H. Park, T. Schenk, C. M. Fancher, E. D. Grimley, C. Zhou, C. Richter, J. M. LeBeau, J. L. Jones, T. Mikolajick, U. Schroeder, *J. Mater. Chem. C* **2017**, 5, 4677.

- [51] R. Materlik, C. Künneth, A. Kersch, *J. Appl. Phys.* **2015**, *117*, 134109.
- [52] R. P. Haggerty, P. Sarin, Z. D. Apostolov, P. E. Driemeyer, W. M. Kriven, *J. Am. Ceram. Soc.* **2014**, *97*, 2213.
- [53] F.-J. Si, W.-J. Lu, F.-L. Tang, *Chin. Phys. B* **2012**, *21*, 076501.
- [54] T. Schenk, *PhD Thesis*, TU Dresden, Germany **2017**.
- [55] J. L. Jones, *Mater. Sci. Eng. B* **2010**, *167*, 6.
- [56] T. Schenk, M. Hoffmann, M. Pešić, M. H. Park, C. Richter, U. Schroeder, T. Mikolajick, *Phys. Rev. Appl.*, under review.
- [57] E. D. Grimley, T. Schenk, X. Sang, M. Pešić, U. Schroeder, T. Mikolajick, J. M. LeBeau, *Adv. Electron. Mater.* **2016**, *2*, 1600173.
- [58] F. G. P. Fengler, M. Pešić, S. Starchich, T. Schneller, C. Künneth, U. Böttger, H. Mulaosmanovic, T. Schenk, M. H. Park, R. Nigon, P. Murali, T. Mikolajick, U. Schroeder, *Adv. Electron. Mater.* **2017**, *3*, 1600505.
- [59] M. E. Lines, A. M. Glass, *Principles and Applications of Ferroelectrics and Related Materials*, Oxford University Press, NY **2001**.
- [60] R. Thomas, V. K. Varadan, S. Komarneni, D. C. Dube, *J. Appl. Phys.* **2001**, *90*, 1480.
- [61] S. Chattopadhyay, P. Ayyub, V. R. Palkar, M. Multani, *Phys. Rev. B* **1995**, *52*, 13177.
- [62] A. K. Tagantsev, M. Landivar, E. Colla, N. Setter, *J. Appl. Phys.* **1995**, *78*, 2623.
- [63] J. M. D. Coey, M. Venkatesan, P. Stamenov, C. B. Fitzgerald, L. S. Dorneles, *Phys. Rev. B* **2005**, *72*, 024450.
- [64] C. D. Pemmaraju, S. Sanvito, *Phys. Rev. Lett.* **2005**, *94*, 217205.
- [65] D. W. Abraham, M. M. Frank, S. Guha, *Appl. Phys. Lett.* **2005**, *87*, 25502.
- [66] W. Zhou, Q. Shi, B. F. Woodfield, A. Navrotsky, *J. Chem. Thermodyn.* **2011**, *43*, 970.
- [67] E. Yurchuk, J. Müller, S. Knebel, J. Sundqvist, A. P. Graham, T. Melde, U. Schröder, T. Mikolajick, *Thin Solid Films* **2013**, *533*, 88.
- [68] M. H. Park, Y. H. Lee, H. J. Kim, T. Schenk, W. Lee, K. D. Kim, F. P. G. Fengler, T. Mikolajick, U. Schroeder, C. S. Hwang, *Nanoscale* **2017**, *9*, 9973.